J Fail. Anal. and Preven. (2010) 10:399–407
DOI 10.1007/s11668-010-9359-2

TECHNICAL ARTICLE—PEER-REVIEWED

Hydrogen Embrittlement on High-Speed Stainless Steel Belts Used for Tin Plating Chip Lead Frame

Yun-Song Gu · Yi Gong · Zhen-Guo Yang

Submitted: 27 April 2010 / in revised form: 30 May 2010 / Published online: 9 June 2010

Abstract The 300 series stainless steels generally exhibit good corrosion resistance in common use. However, a premature fracture event caused by hydrogen embrittlement was encountered on 300 series stainless steels which was used as belt hanging chips in a tin plating process for the chip lead frame. The cause of the fracture was carefully studied. A metallurgical microscope and photoelectric direct reading spectrometer were used to examine the metallographic structures and chemical compositions of the matrix material. A scanning electron microscope and energy disperse spectroscope were also applied to analyze the micro morphologies and micro-area composition of the fracture. Meanwhile, the chemistry and hydrogen content of the process media were inspected by ion chromatography and hydrogen analyzer. In addition, the finite element method was employed to simulate the effect on the belt from the service conditions. The analysis results revealed that the unqualified material selection, the aggressive media, and the inappropriate technological parameters were the main causes of the failure. Furthermore, the mechanisms of hydrogen embrittlement were discussed, and countermeasures and suggestions were put forward.

Keywords Stainless steel belt · Hydrogen embrittlement · Failure analysis

Introduction

Integrated circuits (IC) have wide applications in our daily life, including our use of mobile phones, laptops, electrical appliances, and so on. Actually, the chip lead frame which is installed around the chip for the purposes of supporting the chip, dissipating heat, and connecting exterior circuit, is an important component in IC. To provide for a good weldability between chips and chip lead frames or between the gold wires on frame, electric plating the effective area of chip lead frame is a significant procedure in manufacturing process. However, equipment used in the entire production line, particularly the stainless steel belts that are fixed on a rotational disk to hang the chip lead frames in tin plating process, is frequently subjected to failure events due to the severe service conditions.

The main activities of the tin plating process for chip lead frames are commonly divided into six steps, including electrolytic deburring, deoxidation, activation, electroplating, neutralization, and deplating, seen in Fig. 1. These activities include the use of aggressive solutions and large-density currents in the deoxidation and/or activation steps. Failure events are typically caused by the coupling of the solutions and currents with inappropriate materials selection for the belts. Thus, solution chemistry, current densities, and material choices are the three most serious factors associated with failure and can cause hydrogen embrittlement failure events on the stainless steel belts. The high-pressure washing water (nearly 20 MPa) imposed in the second substep after electrolytic deburring is also an important failure causing process and all six successive and repetitive steps may aggravate any failure extent.

In this case, a failure event was reported occurring on the stainless steel belts used for hanging the chip lead frames of a tin plating production line in one chip manufacturing works in Shanghai. Some stainless steel belts, made of the so-called '304' stainless steel (according to the manufacturer), failed within one month. This lifetime is much shorter than the expected life of longer than six months. Thus, a

Y.-S. Gu · Y. Gong · Z.-G. Yang (✉)
Department of Materials Science, Fudan University,
No. 220 Handan Road, Shanghai 200433,
People's Republic of China
e-mail: zgyang@fudan.edu.cn

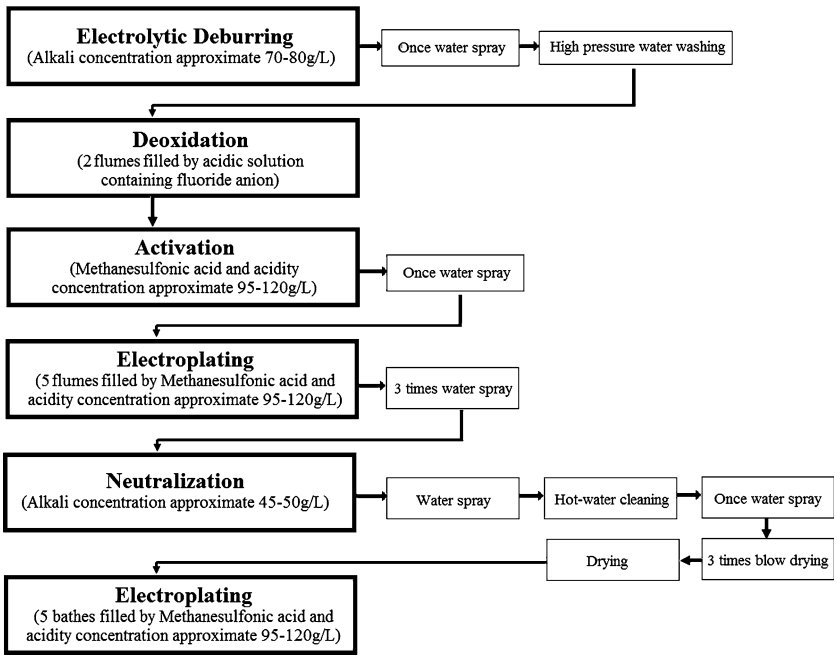

Fig. 1 Process, medium, and concentration of tin plating technics

thorough survey through field investigations and sampling analyses on the causes and the mechanisms of this failure was required to reduce the downtime and resulting increase in production costs. Consequently, ion chromatography (IC) was used for determining chemical composition of plating solution, while hydrogen analyzer, photoelectric direct reading spectrometer, metallurgical microscope (MM), scanning electronic microscope (SEM) were applied to detect the chemical compositions, metallographic structures and macro & micro morphologies of the failured stainless steel belts, respectively. Furthermore, finite element method (FEM) as an auxiliary method was also employed to simulate the stress distribution on the steel belts under high pressure washing water. The analysis results showed that the main cause of this failure was hydrogen embrittlement, which was introduced from the solutions used in deoxidation and electroplating steps. Finally, mechanisms of the failure were discussed and suggestions were proposed, which have significant importance not only in failure prevention for steel belts used under similar service conditions but also in developing a better understanding of hydrogen embrittlement in engineering practice. The service life of stainless steel belts was extended to the normal level by accepting these suggestions.

Experimental Methods and Results

Visual Observation

The different macro morphologies of the original and the failed stainless steel belts are shown in Fig. 2a and b, respectively. Figure 2b indicates that the failed position is the bottom bracket of the belt. Moreover, the flat fracture is a sign of macroscopically brittle failure processes, seen in Fig. 2c.

Matrix Materials Examination

Chemical compositions of three types of the stainless steel belt samples, i.e., the original one, the failed one which used only one month, and the normal one which used longer than 4 months, were inspected by photoelectric direct reading spectrometer. The main content in matrix material is listed in Table 1. It is found that the matrix material of the failure steel belt was 301 stainless steel which has higher carbon content and less chromium than the 304 stainless steel required from design. This contrasts the matrix of the belt used for 4 months which was 316L stainless steel. The 316L steel has an excellent corrosion resistance but a relatively higher cost. Commonly, as metastable austenitic stainless steels [1], both 301 and 304 exhibit a severer hydrogen embrittlement aptitude than stable austenitic stainless steels [2]. This observation suggests that inappropriate materials selection may be one of the failure causes.

In order to judge whether the steel belts were given a surface treatment to increase of corrosion resistance, chemical compositions of the polished original stainless steel belts, and the unpolished one were measured and are listed in Table 1 [3]. It's obvious that both surfaces have the similar chemical compositions, demonstrating that no surface treatment was conducted. Thus, the lack of a required surface treatment to the steel belts is another factor of the failure.

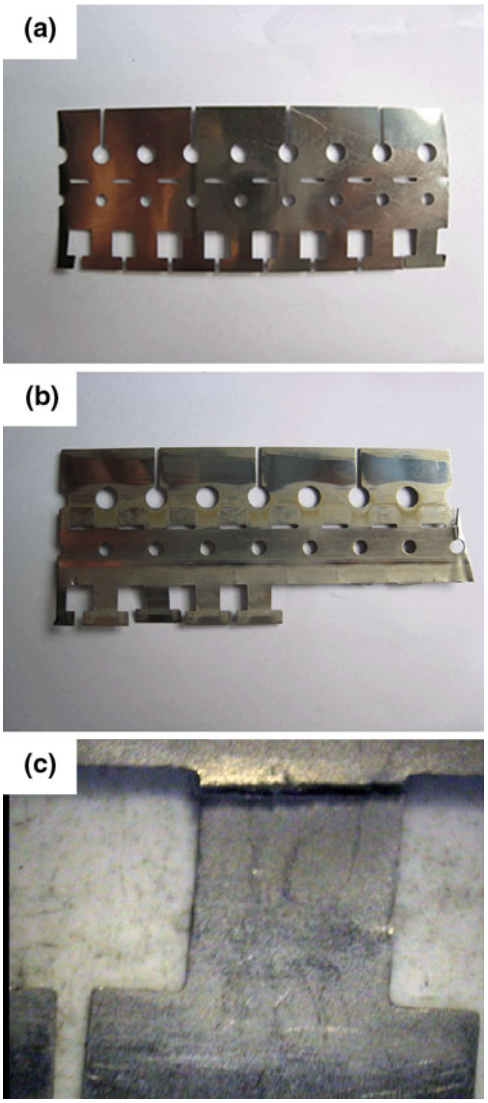

Fig. 2 Macroscopic appearance of stainless steel belt: (**a**) original one, (**b**) fractured one, and (**c**) fracture

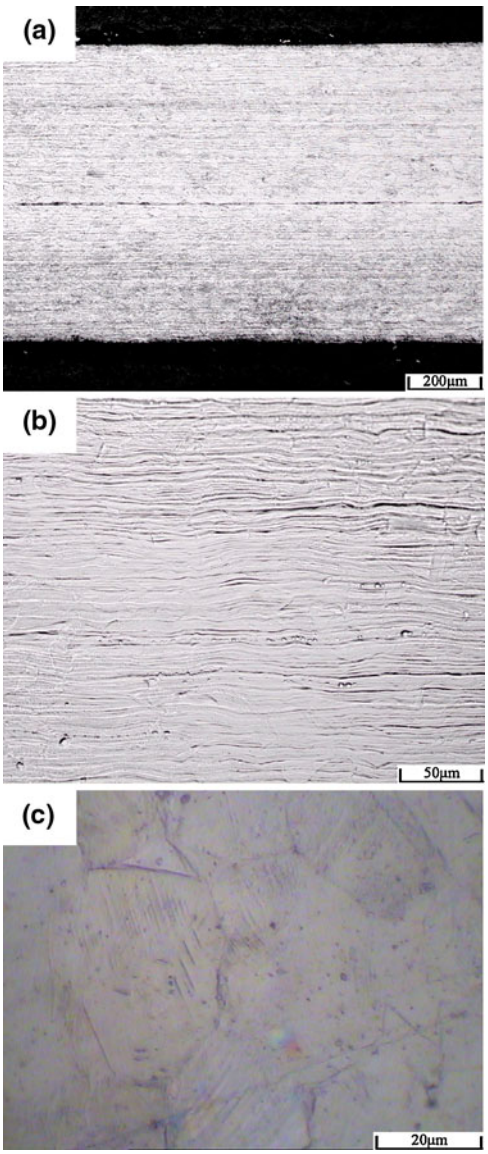

Fig. 3 Metallographic structure of fractured stainless steel belt's cross section: (**a**) cross section 100×, (**b**) center of cross section 500×, and (**c**) surface of stainless steel belt

Table 1 Chemical compositions of original and fractured stainless steel belts (wt.%)

Element	C	Si	Mn	P	S	Cr	Mo	Ni
AISI 301	≤0.15	≤0.75	≤2.00	≤0.045	≤0.030	16.0 ~ 18.0	/	6.00 ~ 8.00
AISI 304	≤0.08	≤0.75	≤2.00	≤0.045	≤0.030	18.0 ~ 20.0	/	8.00 ~ 10.50
AISI 316L	≤0.03	≤1.00	≤2.00	≤0.045	≤0.030	16.0 ~ 18.0	2.00 ~ 3.00	12.00 ~ 15.00
Failure one (polished)	0.1105	0.7246	1.0432	0.0026	0.0317	17.2484	0.1585	6.7737
Original one (polished)	0.1103	0.7223	1.0411	0.0027	0.0320	17.2311	0.1581	6.7831
Original one (unpolished)	0.1092	0.7633	1.0212	0.0007	0.0267	17.0354	0.1602	6.4379
Normal one after 4-month use	0.019	0.719	0.94	0.0034	0.004	16.40	2.17	10.05

It is well known that 300 series stainless steels commonly exhibit austenitic microstructures. However, as it is shown in Fig. 3, metallographic structure of the cross section of the failed stainless steel belt is a mixture microstructure of both austenite and martensite which has a twisted fibrous morphology. Generally speaking, the

existence of martensite, which occurs at the inner part of austenite by means of strain-induced martensitic phase transformations, increases the hydrogen uptake because the hydrogen diffusion coefficient and permeability of martensite is higher than austenite [4]. Therefore, the martensitic transformation products could act as a suitable medium for hydrogen to entry and transport in the stainless steel [5].

Ion Chromatography

Ion chromatography was used to semi-quantitatively analyze the main anions in the solutions that the steel belts encounter, i.e., the deoxidation solution, the electrolytic deburring solution, and the deplating solution. In addition to the sulfate SO_4^{2-} which was detected in all three solutions, the fluoride anion F^- was particularly found in the deoxidation solution, as seen in Fig. 4. Commonly, SO_4^{2-} is a main component in the electroplating solution and is present as sulfuric acid. The F^- is a halide ion that is known inducing corrosion on metals, especially pitting corrosion. However, it has been reported that a relatively high concentration of F^- will provide an inhibiting effect to the pitting corrosion of carbon steels [6]. In this case, the concentration of F^- is 6.4 g/l and may explain why there was no obvious evidence of pitting corrosion on the stainless steel belt.

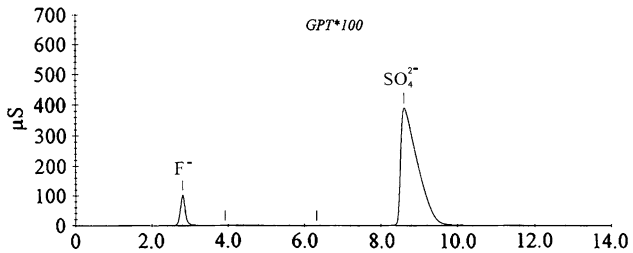

Fig. 4 Chromatographic analysis result of deoxidation solution

Hydrogen Absorption

According to the technological parameters, hydrogen concentration in the original 304 stainless steel belt is 6 ppm, whereas the value for the failed one which used only one month exceeds 17 ppm. The hydrogen absorption analysis thus showed the use had increased the hydrogen content to nearly three times of the normal value. Such an increase in hydrogen may result from hydrogen evolution reactions during the engineering production process and will favor the onset of hydrogen embrittlement.

SEM and EDS Analysis

Surface of Failed Steel Belts

Figure 5 displays the SEM micrographs of the surface of the failed stainless steel belts and compares that surface to the normal surface morphology. Regularly distributed micro cracks and pits can be clearly found in Fig. 5b and c and are absent in Fig. 5a. Additionally, there are linear cracks parallel to the fracture, and some of these cracks

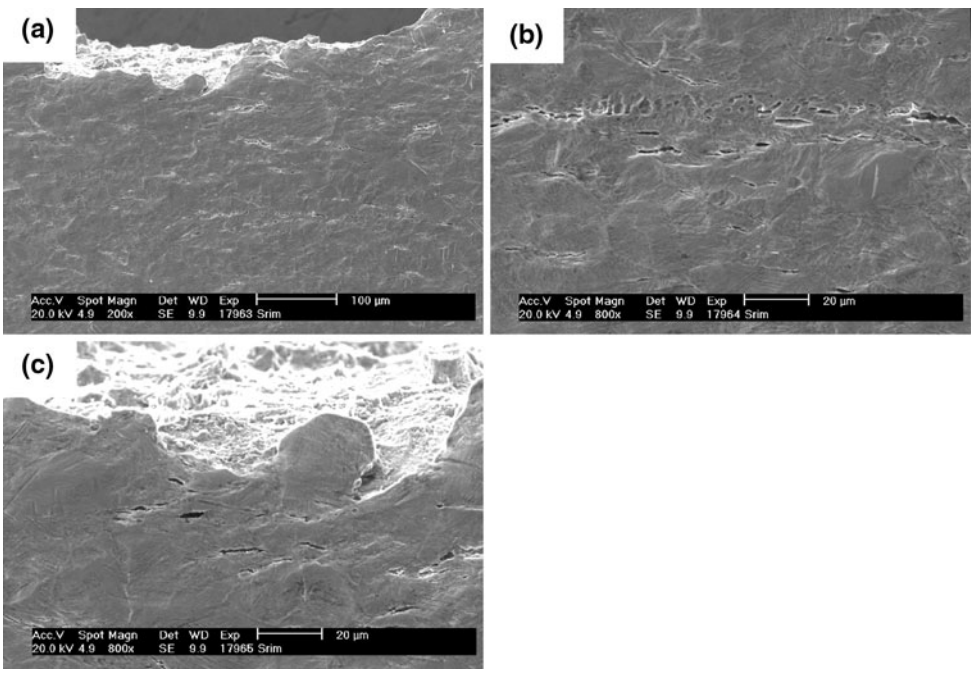

Fig. 5 SEM micrograph of defects in fractured belt bracket surface: (**a**) morphology of belt bracket surface, (**b**) enlarged local region, and (**c**) enlarged side of fracture

have connected to form a larger one. Moreover, a peculiar morphology of step-shaped crack group found on the surface is the typical feature of hydrogen-induced stepwise cracking (HISC). According to the EDS result shown in Fig. 6, it can be seen that no chlorine and fluorine elements were found on the surface of the failed steel belts, which indicates that halide-induced pitting corrosion should not be blamed for the emergence of the pits on the surface. Hence, it can be further identified that pits around the micro cracks were caused by hydrogen blistering (HB). To sum up, all the above observations are relevant to hydrogen embrittlement of the stainless steel belt which reduced its properties and eventually resulted in fracture [7].

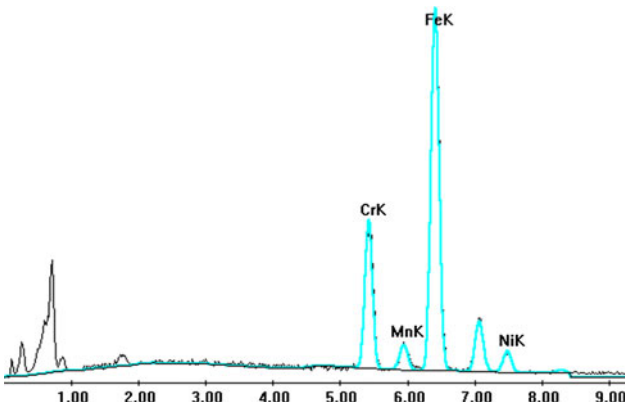

Fig. 6 Result of EDS

Fractograph of Failed Steel Belts

In Fig. 7a, a flat cross section can be observed on the fracture. This fracture topography is generally a sign of macroscopically brittle fracture and is consistent with the failure mechanism of hydrogen embrittlement. Additionally, a long dark strip with even smoother surface is seen on the bottom of the fracture, Fig. 7b. This is a typical morphology of erosion, and then it can be inferred that the ultimate fracture of the steel belts may also involve the high-pressure water washing procedure.

Both obvious cleavage steps and dimples can be found in Fig. 8a. However, the cleavage steps cover most of the cross section, while the dimples were found only in the middle part of the cross section, seen in Fig. 8b. This phenomenon is consistent with fracture of the steel belts by hydrogen embrittlement with the embrittlement process being initiated from the outer surfaces of the belt.

In order to qualitatively analyze the effect from the high-pressure washing water (20 MPa) imposed on the stainless steel belt, finite element method (FEM) software was employed to simulate the stress distribution on the belt after washing. This is actually a two-dimensional (2-D) transient elastic-dynamic analysis [8–10], and the meshed FEM model with element of *PLANE 82* is presented in Fig. 9. The fractured part was further refined for accuracy. Thickness of the belt is 0.5 mm, Poisson ratio and Young's modulus were set as 0.3 and 2.06×10^5 MPa, respectively. Displacement of the left and right sides (except the bracket)

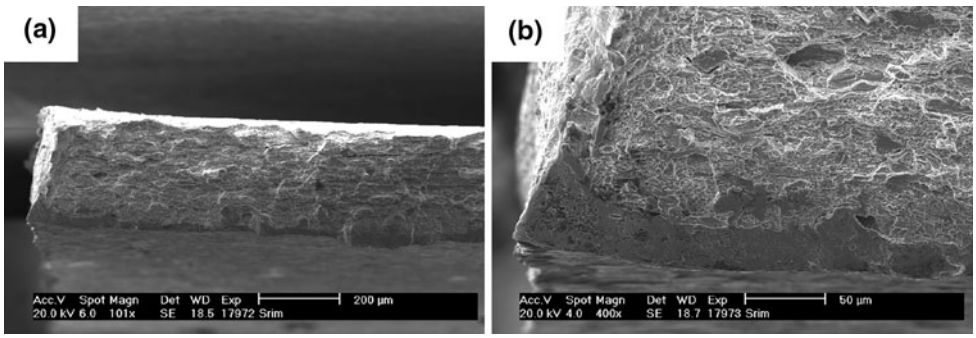

Fig. 7 SEM micrograph of fracture surface of belt bracket: (**a**) facture surface of belt bracket and (**b**) enlarge the left part

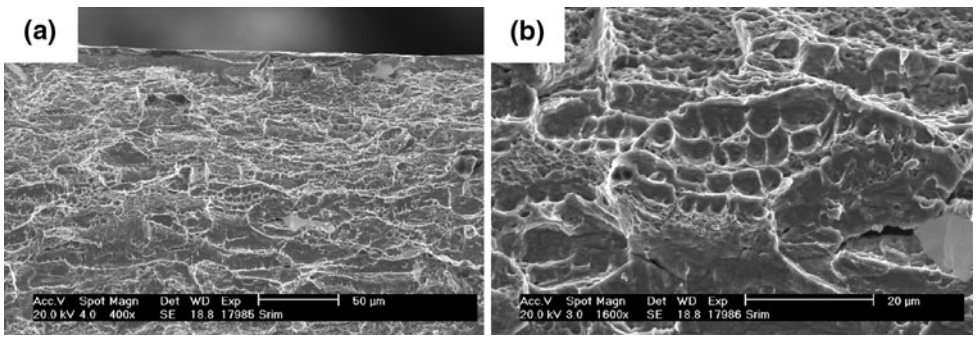

Fig. 8 SEM micrograph of stainless steel belt's fracture: (**a**) expended morphology of stainless steel belt's fracture and (**b**) dimples showing expended direction

of the belt was set zero as the boundary conditions. According to the calculated results summarized in Fig. 10a, the stress concentrates on the corner of the bracket and its maximum value is about 8×10^4 MPa, Fig. 10b. This maximum stress value far exceeds the anticipated yield strength of the stainless steel component and must have contributed to the fracture.

Failure Analysis

It has been concluded that two factors were the primary contributors to the failure process: (1) the use of unqualified materials in the belt and (2) hydrogen embrittlement driven by the aggressive process media. Consequently, further discussion will be conducted on these two aspects.

Materials Selection

It was determined that the matrix material of the stainless steel belt that failed after one-month use was 301 stainless steel. This alloy which has higher carbon content (up to 0.15%) and much lower resistance to hydrogen embrittlement than either 304 or 316L stainless steel. Tama [11] found that the solubility of carbon was very low in steels at room temperature, and was only 0.006% in austenite. This means the carbon existing in these steels has the potential to form carbides such as $M_{23}C_6$, M_7C_3, etc. The higher the carbon content steels the more likely carbides are to be present. Carbides and other inclusions, i.e., manganese sulfide, which are precipitated in the grain boundaries, become failure initiation sites, i.e., the nucleation centers of microvoid nucleation and the development of hydrogen-induced cracks. Although most of cracks are initiated at the MnS inclusions, some researches showed that it is not necessary for HISC to nucleate at such inclusions the observed stepwise crack nucleation sites are typically grain and carbide-matrix interphase boundaries [7]. The introduction of above boundaries in 301 is more than it is in 304 or 316 stainless steels. The selection and use of 301 stainless steel increased the likelihood of HISCs and therefore the probability of failure. Thus, the conclusion can be put forward that inadequate selection of material was one of the main causes of the failure of stainless steel belt. What's more, according to the above analysis, no surface treatment was given to the belt material and the lack of this treatment increased the possibility of failure [12–15].

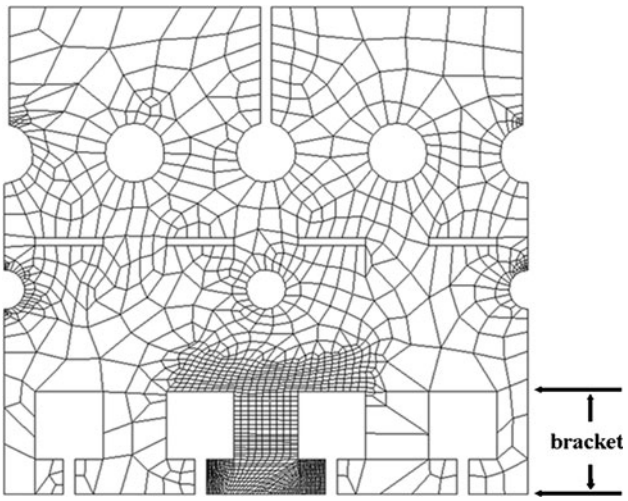

Fig. 9 Meshed FEM model of the stainless steel belt

Hydrogen Embrittlement

Hydrogen Generation

In order to mitigate the hydrogen embrittlement process, sources of the hydrogen in this case must be confirmed. Actually, nearly all the six steps in the tin plating process may bring hydrogen to the stainless steel surfaces. However, most of the hydrogen is generated in deoxidation, activation, and electroplating steps.

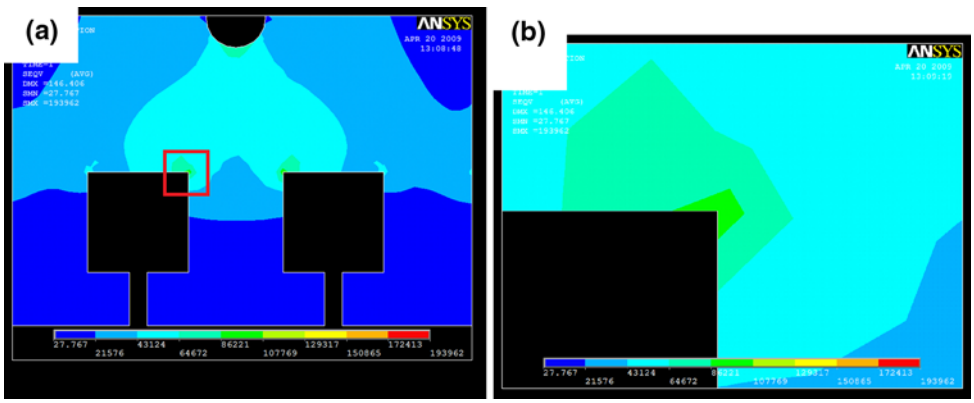

Fig. 10 Stress distribution on the stainless steel after water washing: (**a**) FEM calculated result and (**b**) enlarged view of the bracket's corner

Activation Step The activation bath in this case was smaller than regular bath generally used and the activation time was about 10–12 s compared with only 5 s in the regular bath. Also, the current density per unit area was higher than normal value. Large density current and longer exposure time means that more hydrogen was generated in this step. The quantity of hydrogen depends on the total current passing through the stainless steel belt and hydrogen is given by Faraday's Law [16]:

$$Q = (1 - \eta_k) \cdot \frac{I \cdot t}{96500}$$

In this equation, Q is the generated quantity of hydrogen, η_k is the current efficiency, I is the current, t is the activation time, and 96500 is the Faraday constant. In this step, hydrogen evolution is primary the side reaction, so $(1 - \eta_k)$ almost equals the efficiency of hydrogen generation. In the same section of activation step, the current density is proportional to I. This equation demonstrates that a lot of the hydrogen generated was due to the increased time of activation and larger density current. Additionally, hydrogen evolution in activation step could extend to deoxidation and electroplating steps.

Deoxidation Step Electrolysis pickling is used in deoxidation step and will generate additional hydrogen. Sulfuric acid is used in deoxidation step from IC analysis (Fig. 3). Commonly, there are four main reactions which may take place on the stainless steel belt surfaces when exposed to sulfuric acid.

$$Fe_2O_3 + 3H_2SO_4 \rightarrow Fe_2(SO_4)_3 + 3H_2O \quad \text{(Eq 1)}$$

$$Fe_3O_4 + 4H_2SO_4 \rightarrow FeSO_4 + Fe_2(SO_4)_3 + 4H_2O \quad \text{(Eq 2)}$$

$$FeO + H_2SO_4 \rightarrow FeSO_4 + H_2O \quad \text{(Eq 3)}$$

$$Fe + H_2SO_4 \rightarrow FeSO_4 + 2H \quad \text{(Eq 4)}$$

As the solubility of $Fe_2(SO_4)_3$ is smaller than $FeSO_4$, reaction (1) and (2) are the slow ones comparing with reaction (3) and (4). The surface of stainless steel belt is covered by oxide layer which is rich in Cr_2O_3 and protects the stainless steel surfaces. Therefore, the aforementioned reactions would not take place until the oxide layer was broken. Once the surface passivation layer is broken, the sulfuric acid enters cracks in the layer and reacts with the exposed Fe, Cr, Ni alloy and enlarges and deepens the cracks. The generated hydrogen can enter stainless steel belt through cracks [17].

Electroplating Step As we know, hydrogen evolution reactions occur when the rate of the hydrogen reduction reaction is higher than that of hydrogen oxidation. These two rates are equal in equilibrium reaction. In other words, only when the equilibrium potential of hydrogen electrode's reduction reaction reaches certain over potential value, the hydrogen evolution reaction occur. The differential between hydrogen evolution potential and hydrogen equilibrium potential is called "hydrogen evolution over potential" and η is used to denote it. The value of η is determined by Tafel's equation:

$$\eta = a + b \log j$$

In which, both a and b are constants and the value of $b\log j$ could be ignored in most metals, i.e., the value of η equals a. In acidic solution, the value a is 0.70 for steel, compared with the value of 0.87 for copper and 1.20 for tin. The lower a (i.e., the hydrogen evolution over potential) is, the more easily hydrogen evolution reaction occurs. The reaction formulas are given as follows [18, 19]:

$$\text{Cathodic reaction: } H^+ + e \rightarrow H, \quad H + H \rightarrow H_2 \quad \text{(Eq 5)}$$

and

$$Sn^{2+} + 2e \rightarrow Sn \quad \text{(Eq 6)}$$

$$\text{Anodic reaction: } Sn \rightarrow Sn^{2+} + 2e \quad \text{(Eq 7)}$$

Reaction (5) takes place on the surface of stainless steel belt, and (6) takes place on the surface of chip lead frame.

Hydrogen Embrittlement

Hydrogen atoms usually enter material by means of adsorption and dissociation of hydrogen molecules [20]. It is known that fatigue and hydrogen-induced fracture generally initiates at the material surface [21] and that hydrogen can enter stainless steel surfaces rather than be eliminated by the surface oxide layer. The hydrogen molecules reach the metallic surface and are transported to the crack tip and absorbed. There are two factors involved in this absorption: one is physical adsorption of the hydrogen molecules and the other is chemical absorption of nascent hydrogen (protons) and movement of the nascent hydrogen into the steel (absorption). These two processes can be explained as two key steps, shown in Fig. 11 [22]. Hydrogen molecules must dissociate into two hydrogen atoms in order to enter the stainless steel [23]. Hydrogen atoms penetrate into the belt and are trapped at defects such as carbides, sulfides, and grain boundaries. These trapped hydrogen protons will accumulate and may form H_2 molecules at microvoids inside the steel. After forming H_2 molecules, the hydrogen pressure within the microvoids will increase and may cause blistering and/or bond breaking, i.e., result in hydrogen embrittlement on the material. In fact, hydrogen pressure relates to the hydrogen concentration:

$$C_H = 135\sqrt{p_{H_2}} - \frac{6500}{RT}$$

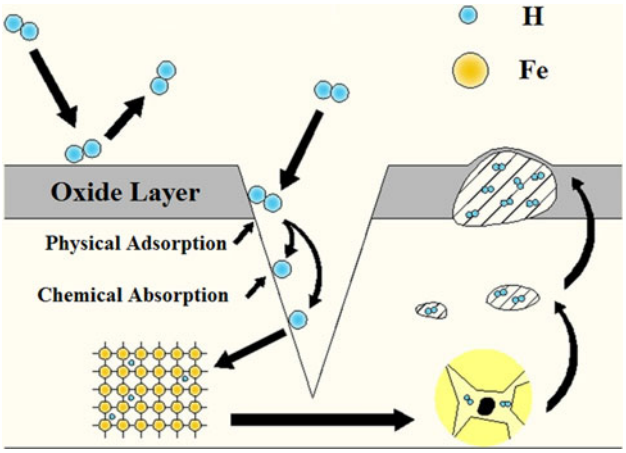

Fig. 11 Main phenomena of hydrogen embrittlement according to Nelson [22]

C_H is the hydrogen concentration in ppm, p_{H_2} is the hydrogen gas pressure in MPa, R is the gas constant, and T is the absolute temperature in K. At room temperature, 1 ppm of dissolved hydrogen can lead to a pressure of 2×10^5 MPa [24]. In this case, the concentration of hydrogen was 17 ppm, so hydrogen embrittlement was possible. Once the hydrogen pressure is high enough to break metallic bonds, micro cracks would be formed to alleviate the pressure, seen in Fig. 5b. After that, newly generated hydrogen could enter the freshly formed surfaces and create another region of H_2 gas pressure. Under this repetitive process, micro cracks propagate and then connect into larger ones, and finally cause macroscopic fracture of the stainless steel belt. Furthermore, based on the FEM results, the high-pressure water washing step will provide the stresses necessary to propagate the micro cracks and cause final fracture.

To sum up, this failure procedure is briefly described. Initially, micro cracks or micropores were engendered by hydrogen embrittlement, and were gradually connected into larger ones. Emergence of cracks caused the strength to decrease. The cracks then propagated both along the axial direction of the belt primarily because of hydrogen accumulations and across the thickness of the belt under the high-pressure washing water. The aggressive acid condition in plating technics may deepen these cracks according to reacting with the exposed steel on the fresh surface of cracks. Thus, a long dark smooth strip can be observed on the edge of the cross section of fracture. With growth of cracks, effective thickness and strength of the steel belt were further reduced. Plastic deformation occurred on the steel belts under high-pressure water washing, and dimples were simultaneously generated in the mid of the belt along thickness. Eventually, the steel belt fractured, and a small area of dimples was left in the middle part of the cross section of fracture.

Conclusion and Suggestion

(1) The unqualified selection of the belt matrix material as 301 stainless steel, an alloy whose corrosion resistance is inferior to 304 and 316 stainless steel, coupled with the lack of a protective surface treatment, was one of the main causes of the failure.
(2) On the failed steel belt, localized defects as micro cracks, hydrogen blisters, and erosion traces were the major failure morphologies. These surface/fracture features which resulted from hydrogen uptake during service and ultimately hydrogen embrittlement. The high pressure washing also caused an erosive effect that contributed to the failure.
(3) The hydrogen that permeated into the stainless steel belt was introduced primarily from the aggressive solutions applied in the activation, deoxidation, and electroplating steps of the tin plating process.
(4) Inappropriate technological parameters in activation and deoxidation steps, and especially the high-pressure washing water in the washing step after electrolytic deburring, were the two aggravating factors in the failure. The inappropriate parameters accelerated the rate of hydrogen evolution and consequently aggravated hydrogen embrittlement while the high pressure washing facilitated propagation of micro cracks on the steel belts and resulted in the ultimate fracture.

Two suggestions are given to mitigate the observed failure process:

(1) Materials with superior corrosion resistance such as 316L stainless steel or duplex stainless steel are suggested as replacements for the 301 and even the 304 stainless steel as the belt's matrix materials.
(2) Technological parameters for the tin plating process must be optimized. The current density during activation and deoxidation steps, and pressure of the washing water should be appropriately reduced.

Acknowledgments The work was supported by both Advanced Semiconductor Engineering (ASE) Group and Shanghai Leading Academic Discipline Project (Project Number: B113).

References

1. Shanghai Jiao Tong University, Analysis of Metal Fracture Surface. National Defense Industry Press (1979) (in Chinese)
2. Han, G., He, J., Fukuyama, S., Yokogawa, K.: Effect of stain-induced martensite on hydrogen environment embrittlement of sensitized austenitic stainless steels at low temperatures. Acta Mater. **46**(13), 4559–4570 (1998)
3. Ji, G.: World Standard Steel Handbook. Standards Press of China (2004) (in Chinese)

4. Kuromoto, N.K., Guimarães, A.S., Lepienski, C.M.: Superficial and internal hydrogenation effects on the fatigue life of austenitic steels. Mater. Sci. Eng. A **381**(1–2), 216–222 (2004)
5. Perng, T.P., Altstetter, C.J.: Hydrogen permeation and diffusion in cryoformed AISI 301 stainless steel. Scripta Metall. **18**(1), 67–70 (1984)
6. Singh, D.D.N., Ghosh, R., Singh, B.K.: Fluoride induced corrosion of steel rebars in contact with alkaline solutions, cement slurry and concrete mortars. Corr. Sci. **44**(8), 1713–1735 (2002)
7. Ju, C.P., Rigsbee, J.M.: The role of microstructure for hydrogen-induced blistering and stepwise cracking in a plain medium carbon steel. Mater. Sci. Eng. **74**(1), 47–53 (1985)
8. Wang, Y.-F., Yang, Z.-G.: Finite element analysis of residual thermal stress in ceramic-lined composite pipe prepared by centrifugal-SHS. Mater. Sci. Eng. A **460–461**, 130–134 (2007)
9. Wang, Y.-F., Yang, Z.-G.: A coupled finite element and meshfree analysis of erosive wear. Tribol. Int. **42**(2), 373–377 (2009)
10. Wang, Y.-F., Yang, Z.-G.: Finite element model of erosive wear on ductile and brittle materials. Wear **265**(5–6), 871–878 (2008)
11. Folkhard, E.: Welding Metallurgy of Stainless Steels. Chemical Industry Press (2004) (in Chinese)
12. Wang, C.Q., Yu, Y., Fang, Y., Li, T.J.: In situ observation of carbide precipitation and dissolution in strip cast 304 stainless steel. J. Iron Steel Res. **19**(9), 42–46 (2007) (in Chinese)
13. Bungardt, K., Kunze, E., Horn, E.: Untersunchungen über den aufbau des systems eisen-chrom-kohlenstoff. Arch Eisenbüttenwes **29**, 193–203 (1958)
14. Ji, L.-N., Yang, Z.-G., Liu, J.-S.: Failure analysis on blind vias of PCB for novel mobile phones. J. Fail. Anal. Preven. **8**(6), 524–532 (2008)
15. Gong, Y., Cao, J., Meng, X.-H., Yang, Z.-G.: Pitting corrosion on 316L pipes in terephthalic acid (TA) dryer. Mater. Corros. **60**(11), 899–908 (2009)
16. Masuku, E.S., Mileham, A.R., Hardisty, H., Bramley, A.N., Johal, C., Detassis, P.: A finite element simulation of the electroplating process. CIRP Ann. Manuf. Tech. **51**(1), 169–172 (2002)
17. An, M.Z.: Electroplating Theory and Technology. Harbin Institute of Technology Press (2004) (in Chinese)
18. Chemical Machinery Research Institute of Ministry of Chemical Industry: Manual of Corrosion and Protection. Chemical Industry Press (1989) (in Chinese)
19. Li, D.: Electrochemical Theory (Rev. ed.). Beijing University of Aeronautics and Astronautics Press (1999) (in Chinese)
20. Michler, T., Naumann, J.: Coatings to reduce hydrogen environment embrittlement of 304 austenitic stainless steel. Surf. Coat. Technol. **203**(13), 1819–1828 (2009)
21. Borchers, C., Michler, T., Pundt, A.: Effect of hydrogen on the mechanical properties of stainless steels. Adv. Eng. Mater. **10**(1–2), 11–23 (2008)
22. Nelson, H.G.: Testing for Hydrogen Environment Embrittlement: Primary and Secondary Influences, Hydrogen Embrittlement Testing, pp. 152–170. ASTM Special Technical Publication (1974)
23. Ogorodnikova, O.V.: Comparison of hydrogen gas-, atom- and ion-metal interactions. J. Nucl. Mater. **277**(2–3), 30–42 (2000)
24. Woodtli, J., Kieselbach, R.: Damage due to hydrogen embrittlement and stress corrosion cracking. Eng. Fail. Anal. **7**(6), 427–450 (2000)